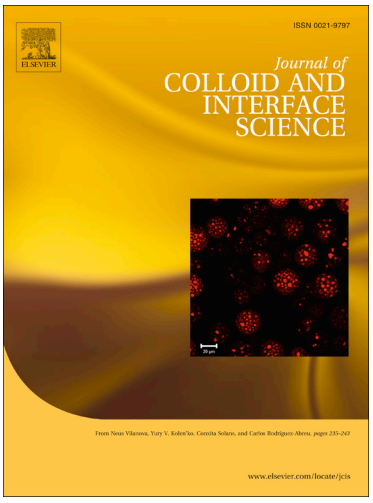

Regular Article

The Role of Adsorbate Size on Adsorption of Ne and Xe on Graphite

Luisa Prasetyo, Kim Q. Loi, Shiliang (Johnathan) Tan, D.D. Do, D. Nicholson

PII: S0021-9797(18)30347-3
DOI: https://doi.org/10.1016/j.jcis.2018.03.091
Reference: YJCIS 23441

To appear in: *Journal of Colloid and Interface Science*

Received Date: 13 February 2018
Revised Date: 25 March 2018
Accepted Date: 26 March 2018

Please cite this article as: L. Prasetyo, K.Q. Loi, S. (Johnathan) Tan, D.D. Do, D. Nicholson, The Role of Adsorbate Size on Adsorption of Ne and Xe on Graphite, *Journal of Colloid and Interface Science* (2018), doi: https://doi.org/10.1016/j.jcis.2018.03.091

The Role of Adsorbate Size on Adsorption of Ne and Xe on Graphite

Luisa Prasetyo, Kim Q. Loi, Shiliang (Johnathan) Tan, D. D. Do* and D. Nicholson
School of Chemical Engineering
University of Queensland
St Lucia, QLD, 4072
Australia

Abstract

We have carried out an extensive grand canonical Monte Carlo simulation to investigate the adsorption of neon and xenon on graphite. The adsorbate collision diameters of neon and xenon are smaller and greater respectively, than the commensurate graphite lattice spacing $\lambda = \left(\sqrt{3} \times \sqrt{3}\right) R30^0$ of 0.426 nm. Simulated isotherms and isosteric heats were obtained using a graphite model that has been shown to describe successfully the adsorbate transitions for krypton, methane and nitrogen [1], which have collision diameters close to λ. Neon does not exhibit commensurate (*C*) packing because the gain in the intermolecular potential interactions in the incommensurate (*IC*) packing when molecules move away from carbon hexagon centres, does not compensate for the increase in the solid-fluid potential energy. Xenon, on the other hand, exhibits *IC* packing because its molecular size is greater than λ. Nevertheless, at a sufficiently high chemical potential, the first layer of xenon changes from the *IC* to *C* packing (in contrast to what is observed for krypton, nitrogen and methane). This transition occurs because the decrease in the xenon intermolecular interactions is sufficiently compensated by the increase in the solid-fluid interaction, and the increase in the fluid-fluid interactions between molecules in the first layer and those in the second layer. This finding is supported by the X-ray diffraction study [2, 3].

Keywords: Adsorption; neon; xenon; graphite; commensurate packing; transition; simulation

* Author to whom all correspondence should be addressed, Email: d.d.do@uq.edu.au

Graphical abstract:

Snapshot of Xe adsorption on the new graphite model at 65K for different loadings:

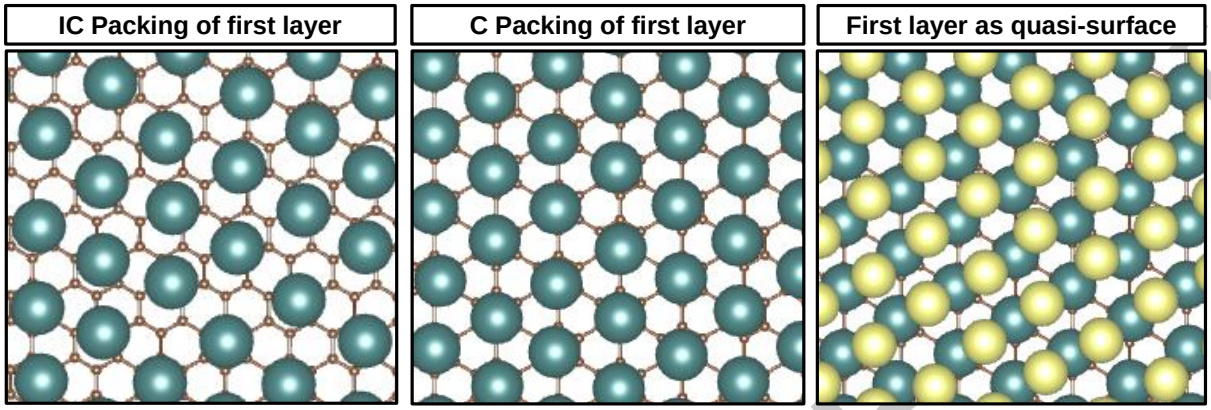

Highlights

- Correct description of the transition from fluid to incommensurate (*IC*) packing for neon
- For xenon, the transition from fluid to incommensurate (*IC*), followed by commensurate (*C*) packing
- The *IC*-to-*C* transition of xenon is opposite to the *C*-to-*IC* transition observed with Kr, N_2, CH_4
- The graphite model accounts for corrugation and anisotropy in polarizability
- Characteristic curve of the isosteric heat versus loading as a function of temperature

1 Introduction

The adsorption of simple gases on graphite has been extensively studied, including Xe [4-7], Ne [8-10], Kr [5, 11-13], Ar [14-16], N_2 [16-18], the oxides of carbon [19, 20] and hydrocarbons, including CH_4 [21, 22], C_2H_4 [23, 24] and benzene [25]. A phenomenon of interest is the ordering transitions of the adsorbate in the monolayer coverage region. These transitions are complex functions of the size and shape of the adsorbate and temperature, as well as the interplay between the adsorbate-adsorbate interaction and the adsorbate-adsorbent interaction. In many simulation studies, the adsorbent is represented by the 10-4-3 continuum model (with Crowell-Steele molecular parameters for the carbon atom in a graphene layer) to describe the interactions between adsorbate molecules and graphite. However, this model is unable to show the experimentally observed commensurate structure of the first layer for simple adsorbates [34-36]. For example, it fails to describe the sub-step in the experimental isotherm of nitrogen at its boiling point (77K) and the corresponding cusp and spike in the plot of the isosteric heat versus loading [1, 26].

Recently we proposed a model for graphite [1, 27], which goes beyond the homogeneous model [28], and achieves better agreement between simulation results and experimental data, particularly the transition from the commensurate (*C*) to incommensurate (*IC*) packing (*Figure* 1). The *C*-packing has a $\left(\sqrt{3}\times\sqrt{3}\right)R30^0$ lattice spacing of 0.426 nm and an adsorbate density of 10.56 μmol/m^2, and the *IC* structure has 2D-hexagonal packing of adsorbate molecules and the adsorbate density depends on the size of the adsorbate.

The new model takes into account:

1. The energetic corrugation parallel to the adsorbent surface, due to the discrete configuration of carbon atoms.
2. The difference between the polarizabilities of a carbon atom in graphite, parallel and normal to the graphene surface.
3. The difference in the interlayer spacing between the top two graphene layers and that of the underneath layers.
4. The smaller collision diameter and greater well depth of interaction energy function for a carbon atom in the outermost layer, and those in the inner layers.

We designate this new graphite model as the corrugation-anisotropy (*CA*). It has recently been demonstrated that it can give excellent agreement with the various transitions in the

adsorption isotherms of N_2 [1], Ar [27], Kr and CH_4, as well as the cusp and spike in the plots of the isosteric heat versus loading.

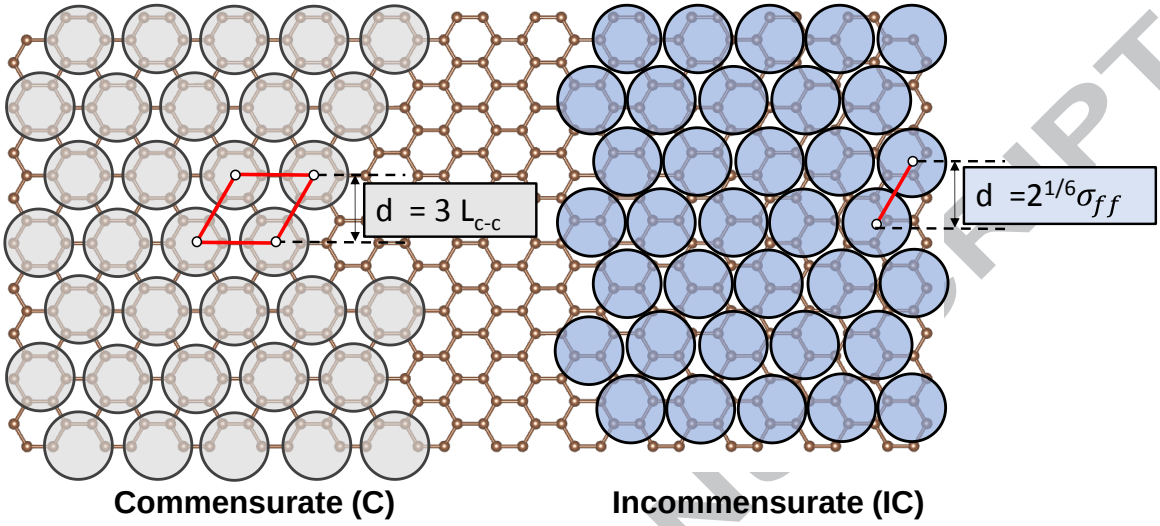

Figure 1 – A schematic diagram of the commensurate and incommensurate packing of single-site molecules on a graphite surface (LC-C is the carbon-carbon bond length)

Other adsorbates from our previous studies (Kr, CH_4, and N_2) have intermolecular separations at the *LJ* potential minimum ($2^{1/6}\sigma_{ff}$) that are less than the commensurate lattice spacing of 0.426 nm, and therefore can form *C* packed layers. Argon, with a minimum separation far less than the commensurate distance is an exception. The potential barrier height between hexagon sites is insufficient to overcome the decrease in the fluid-fluid interactions for argon and therefore argon does not form a commensurate layer [27].

To complete our study of the transitions in the adsorption of noble gases on graphite, this work focuses on the adsorption of xenon and neon, which have, respectively, very strong and very weak interactions with graphite (*Figure* 2), but also have molecular diameters that are much smaller and much larger than the commensurate distance.

Adsorption of xenon on exfoliated graphite has been extensively studied by Thomy and Duval [4, 5] for temperatures in the range 97-117 K and by Suzanne *et al.* [6, 7] for a lower range of temperatures 85-102 K. The reported experimental 2D-triple-point and critical temperatures are 100 K and 117 K, respectively (see *Table 1*). The isotherms of Thomy and Duval exhibit first-order transitions from gas to liquid (*G*-*L*) and liquid to solid (*L*-*S*), while those of Suzanne *et al*. exhibit a first order transition from gas to solid (*G*-*S*). The separation

between a pair of xenon molecules at the *LJ* potential minimum is $2^{1/6}\sigma_{ff} = 0.438$ nm which is greater than the *C*-spacing of 0.426 nm between alternate C hexagons. The solid-solid transition in the first adsorbate layer of xenon is therefore from *IC*-packing to *C*-packing [2, 29], which is in the opposite direction to the 2D solid transitions for krypton, nitrogen and methane. At sufficiently low temperatures, the *IC*-to-*C* transition in xenon occurs before the onset of adsorption in the second layer [30-32]. However, there is lack of agreement among experimental measurements about the threshold temperature above which the *C* solid is not observed before the onset of second layer; 62.5K was reported from THEED studies [30] and 73K from high-resolution synchrotron X-ray diffraction [33, 34]. At higher temperatures, the *IC*-*C* transition in the first adsorbate layer occurs at loadings after the second layer has been formed [2, 3].

In contrast to xenon, adsorption of neon on graphite exhibits a commensurate structure only at temperatures below 5K [35], where the entropy effect is almost negligible. However, at temperatures above 10K, neon behaves similarly to argon and its isotherms exhibit G-L and L-S transitions [9, 10]. The solid is an *IC*-packing, as shown experimentally by LEED [8].

In view of the controversial reports in the literature for neon and xenon adsorption on graphite, we have employed our revised potential function to re-investigate this system. The interaction strength and size of these two molecules lie at opposite extremes of the simple adsorbates previously studied (*Figure* 2). We have completed our study of the adsorption of simple gases on graphite by presenting the characteristic curves of the isosteric heat versus loading as a function of temperature.

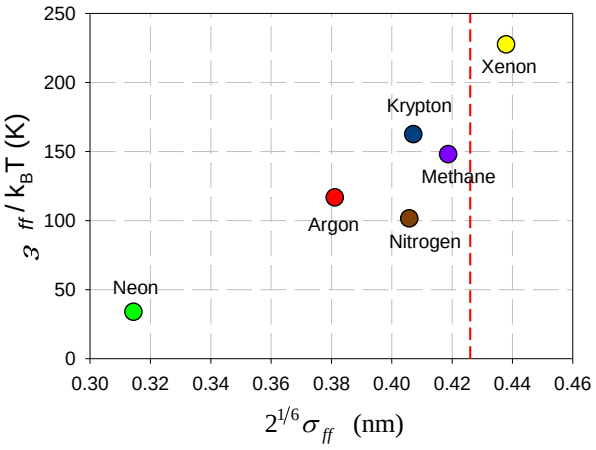

Figure 2 – Plot of the distance at which the intermolecular potential is minimum $\left(2^{1/6}\sigma_{ff}\right)$ versus the reduced well-depth of the interaction energy ε_{sf}/k_B of noble gases, nitrogen [36] and methane. The vertical red dashed

line is the commensurate distance of 0.426 nm. Only krypton, methane and nitrogen experience a *C-IC* ordering transition while argon and neon can only form an *IC* packing and xenon experiences an *IC-C* transition.

2 Theory

2.1 Grand Canonical Monte Carlo (*GCMC*) Simulations

In the *GCMC* simulations, we used 100,000 cycles for low loadings, 500,000 cycles for high loadings and 1 million cycles for loadings at each isotherm point across the *IC-C* transition for both equilibration and sampling stages. Each cycle consisted of 1000 attempted displacement, insertion and deletion moves, chosen with equal probability. In the equilibration stage, the maximum displacement step length was initially set as 2 nm, and was adjusted at the end of each cycle to give an acceptance ratio of 20%. The lengths of the simulation box in the *x*- and *y*- directions parallel to the graphite surface were $\left(30\times 15\sqrt{3}\right)a_0$ to ensure the periodicity of the graphite surface, where a_0=0.246 nm is the graphite lattice constant. The dimension in the *z*-direction was 2 nm. Periodic boundary conditions were applied at the boundaries in the *x*- and *y*-directions and a hard wall was positioned at z=2 nm and the carbon atom centres in the outermost graphene layer of the graphite were positioned at z=0.

2.2 Meso-Canonical Ensemble (*MCE*) Simulations

A two-volume *NVT* scheme [37, 38], which is based on the gauge cell method proposed by Neimark and Vishnyakov [39], was used to obtain the isosteric heats during the phase transition. The system comprises two boxes; one is the adsorption system and the other is a gas reservoir with a suitable cubic dimension to control fluctuations. The linear dimensions of the cubic gas reservoir for the adsorption of Xe at 65K and 105 K are 600nm and 7nm, respectively. Molecules are allowed to exchange between the two boxes. At least 100,000 cycles were used in both the equilibration and sampling stages with each cycle consisting of 1000 attempted displacements or exchanges between boxes chosen at randomly with equal probability. The x- and y-dimensions of the adsorption box were set to be the same as the dimensions used in the *GCMC* simulations. The excess chemical potential was determined using the Widom insertion method [40] and the pressure was calculated via the virial equation.

2.3 Fluid-Fluid and Solid-Fluid Potentials

Fluid-Fluid Potential

The interaction between two adsorbate molecules, the fluid-fluid (*FF*) interaction, was described by the 12-6 Lennard-Jones (*LJ*) equation. The intermolecular parameters for noble gases are given in *Table* 1. They were chosen because of they give an excellent description of the vapour-liquid equilibrium.

Table 1: Lennard-Jones Molecular Parameters of noble gases.

Species	σ (nm)	ε_{ff}/k_B (K)	$2D\text{-}T_t$ (*) (K)	$2D\text{-}T_c$ (*) (K)
Ne	0.2801[41]	33.921[41]	13.6[42]	15.8[42]
Ar	0.33952[41]	116.79[41]	47.2[43]	58[43]
Kr	0.3685[41]	164.4[41]	84.8[4]	86[4]
Xe	0.3901[41]	227.55[41]	100[4]	117[4]

(*) experimental values

Solid-Fluid Potential

The structure and properties of the new graphite model are illustrated in *Figure 3*. The solid adsorbent was modelled as a stack of graphene layers which are infinite in the *x*- and *y*-directions parallel to the surface. The solid-fluid (*SF*) interaction with the outer graphene layer was described by the 10-4 potential while the interaction with the remaining solid was described by the 10-4-3 equation [28] (with the implicit assumption of equal interlayer spacing between the graphene layers. Note that the spacing between the outer two graphene layers is different from that for inner layers). The corrugation in the *SF* interaction between a molecule and the outermost layer followed the equation given by Kim and Steele [44]. The carbon atom density ρ_s was 38.2/nm^2 for all layers. The cross-collision diameter σ_{sf} and the reduced well-depth ε_{sf}/k_B of the *SF* interactions were calculated with the Lorentz-Berthelot mixing rule.

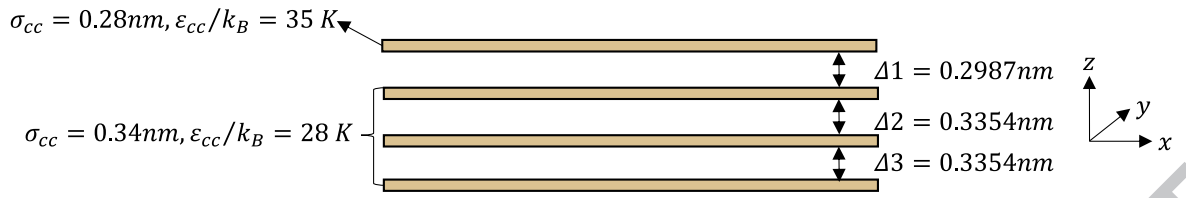

Figure 3 - Schematic illustration of the graphene layers. Top layer is modelled as an energetically corrugated surface, and the underlying layers are modelled as equally spaced homogeneous graphene surfaces.

The energetic corrugation of the *SF* potential function was modified to account for the difference in the carbon atom polarizability parallel to the surface and normal to the surface (Carlos and Cole [45, 46]; Nicholson [47]). This anisotropy enhances the energetic corrugation, and is characterised by two parameters γ_A and γ_R in the Carlos and Cole model [46]. The parameter γ_A comes from the product of the dipole coupling tensors that appear in the calculation of the dispersion force term, and depends on the ratio of the polarizability components of the polarizability tensor. A value of $\gamma_A = 0.4$ was found, based on the graphite dielectric properties [46]. This value was used for both neon and xenon in this work. The parameter γ_R, however, does not have a physical basis and was taken as a fitting parameter; for example, Carlos and Cole [45, 46] found that a value of γ_R = -0.29 gave good agreement for He beam scattering experiments. In this work, the value $\gamma_R = 0$ was chosen for Xe, because it provides a corrugation energy ΔE_{corr} similar to the value used by Bruch *et al*. [29] (details are given in *Appendix* B). For neon, the characteristics of the 2D solid phase of the monolayer are insensitive to the value of γ_R, and we chose $\gamma_R = 0$ for consistency with xenon. To show the difference between the *SF* potential calculated with the current model and the 10-4-3 potential model, we present plots of their z-dependence in *Figure 4*.

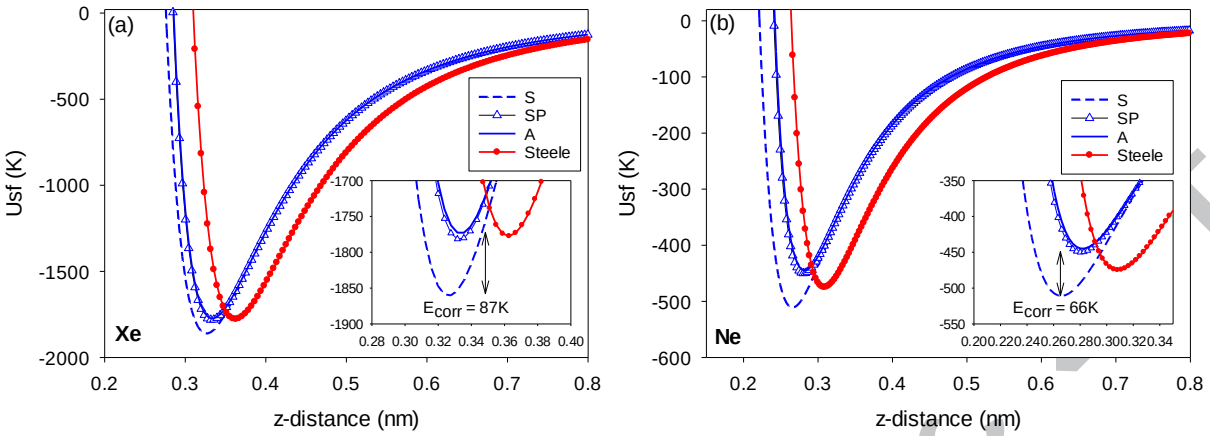

Figure 4 - Comparison between the *SF* energy profile of: (a) xenon and (b) neon with the 10-4-3 potential model and the new graphite model with anisotropy ($\gamma_A = 0.4$, $\gamma_R = 0$). *S* refers to the position of the atom at the centre of carbon hexagon and *SP* and *A* to the position of the adsorbate between two carbon atoms and on top of a carbon atom, respectively.

The thermodynamic properties, *i.e.* surface excess, isosteric heat, local density distribution and radial distribution, of our simulations are defined in *Appendix* A.

3 Results and Discussion

3.1 Adsorption of Xenon on graphite

The simulated isotherms for xenon adsorption on graphite using the new graphite model are shown in *Figure* 5. These isotherms show that the 2D-triple point of the first layer, at a surface excess coverage of 9.77 μmol/m^2, is between 80K and 90K, and the 2D-critical point is between 110K and 120K (in agreement with 117K as reported by Thomy and Duval [4]). The isotherms exhibit a gas to solid transition for temperatures below the 2D-triple point, gas-liquid-solid transitions for temperatures between the 2D-triple and critical points, and a supercritical fluid-solid transition for temperatures greater than the 2D-critical point. We chose 65K and 105K for detailed analysis because the first adsorbate layer reaches *C* packing before the onset of the second layer at 65K, and at 105K the first adsorbate layer reaches *C*-packing after the second layer has been formed.

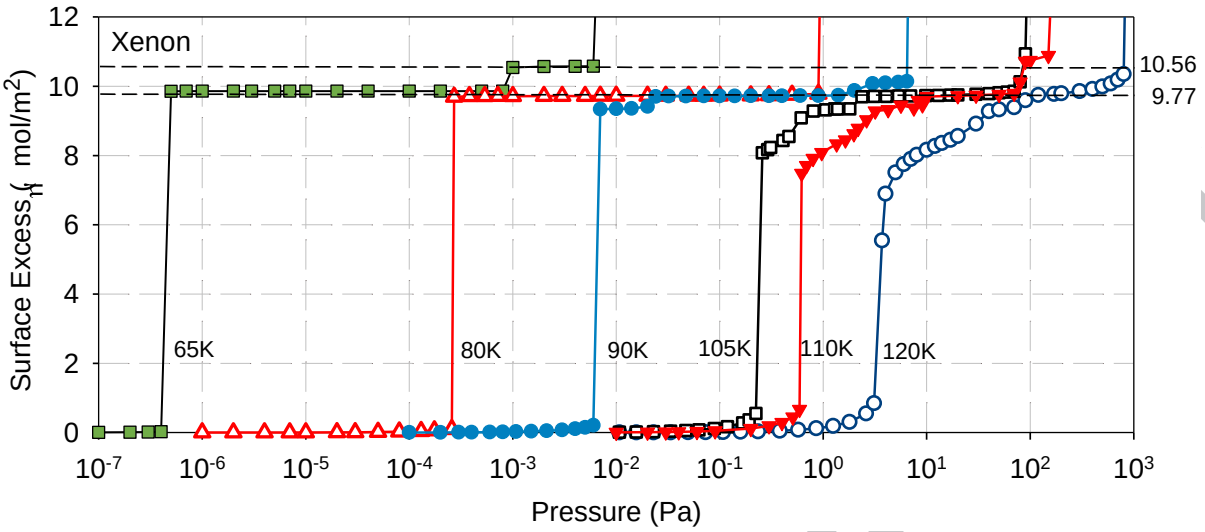

Figure 5 – Simulated xenon adsorption isotherms with the new graphite model for 65K-120K

3.1.1 Adsorption of xenon at 65 K

The adsorption of xenon on graphite at 65K, which is far below the 2D-triple point, is used as a reference because the experimental results exhibit an *IC*-*C* transition before the onset of the second layer [2, 3]. *Figure 6* presents the simulated isotherms for both the homogeneous model and the corrugation-anisotropy (*CA*) model. The *IC*-*C* transition, as observed experimentally, is successfully reproduced with the *CA* model, but the homogeneous model fails.

With the *CA* model, the first layer of xenon undergoes a 2D condensation from a gas-like state to a solid-like state at a surface excess coverage of 10 μmol/m^2, in perfect agreement with the theoretical *IC* density. This is followed by a transition to the *C* packing (once again in perfect agreement with the theoretical *C* density of 10.56 μmol/m^2) before the onset of the second layer. This behaviour is confirmed by the X-ray experimental data [33, 34].

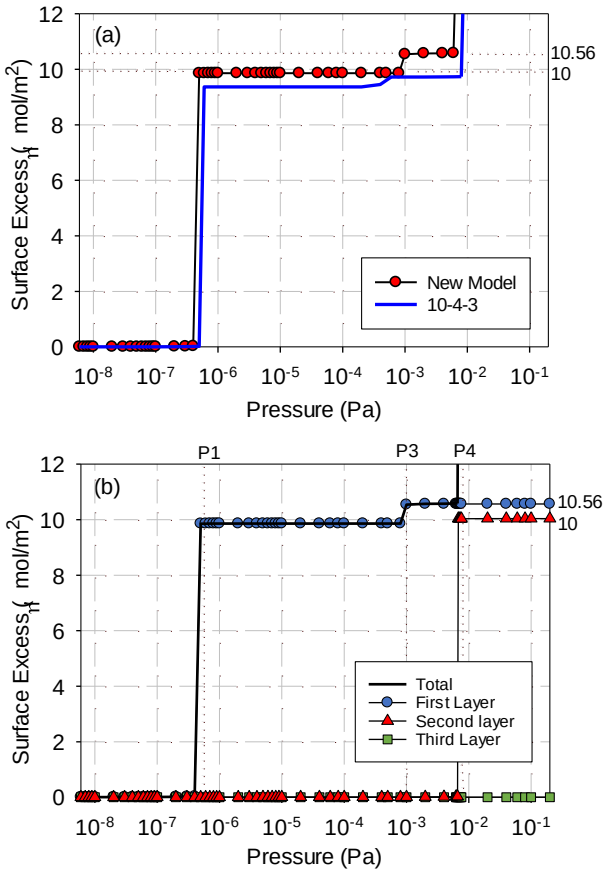

Figure 6 - (a) Isotherm of xenon at 65K: comparison between the *CA* model and the homogeneous 10-4-3 model, (b) isotherms for the first, second and third layers of xenon at 65K obtained with the *CA* model.

The simulated isotherm was decomposed into contributions from the first, second and third layers as shown in *Figure* 6b, which confirms that the first adsorbate layer achieves *C* packing before the onset of the second layer. Interestingly, the formation of the second layer occurs by a 2D-condensation to form a perfect *IC* packing at 10 µmol/m^2, even though the first adsorbate layer has already reached *C*-packing (*CP*) at the higher density of 10.54 µmol/m^2 (*Figure* **7**). This is consistent with the experimental result [31, 33], and indicates that the solid-fluid potential does not play a part in structuring the second layer, where the *CP* structure is determined by the adsorbate-adsorbate interactions.

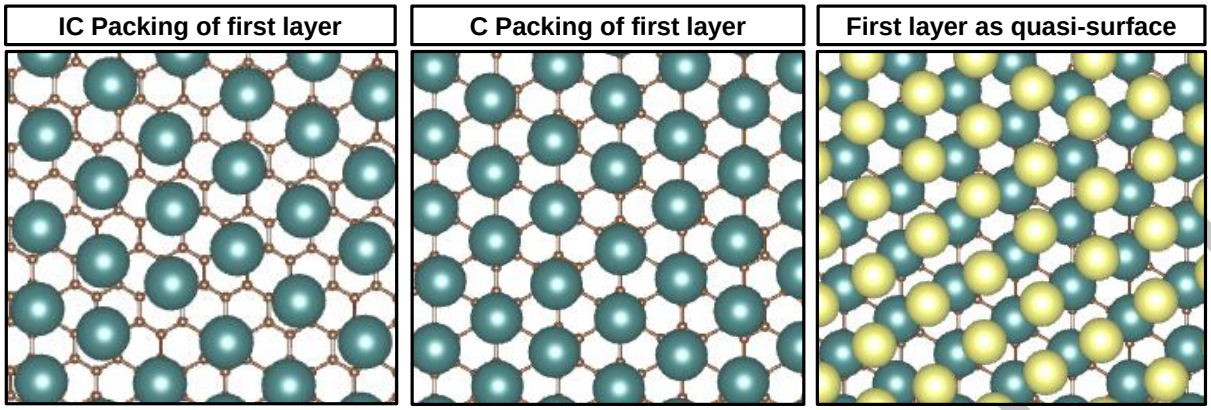

Figure 7 - Top view of the snapshots of xenon molecules on graphite surface at 65K at the *Points P1*, *P3* and *P4* in *Figure* 6 (xenon molecules in the second layer are coloured yellow).

To better understand the adsorption mechanism during the transition, plots of isosteric heat and its contributions from solid-fluid (*SF)* and fluid-fluid (*FF)* interactions versus loading, are shown in *Figure 8*a, b, c. To see more clearly the behaviour of the isosteric heat across the transitions, we have also plotted it as a function of pressure in *Figure 8*d, e, and f. The transition from *IC*-packing to *C*-packing in the first adsorbate layer, before the onset of second layer adsorption, can be seen in *Figure 8*a. The isosteric heat at zero loading $q_{st}^{(0)}$, is 15kJ/mol (which is the same as the value obtained from direct Monte Carlo integration [48, 49]) and increases in the gas-like state as the number of neighbouring molecules increases. The 2D-condensation, corresponding to the *G*-*S* transition, is seen as a discontinuity in the heat curve, with a constant isosteric heat at around 20.5 kJ/mol across the transition, obtained by a meso-canonical ensemble (*MCE*) simulation. The addition of 5.5 kJ/mol to the zero coverage heat comes from the *FF* interactions. Since the pairwise interaction energy of a pair of xenon molecules is 1.89 kJ/mol, this suggests that the 2D-condensation occurs by boundary growth of the *IC*-solid in which each new molecule interacts with three molecules at the boundary of a growing cluster as shown in *Figure* 9.

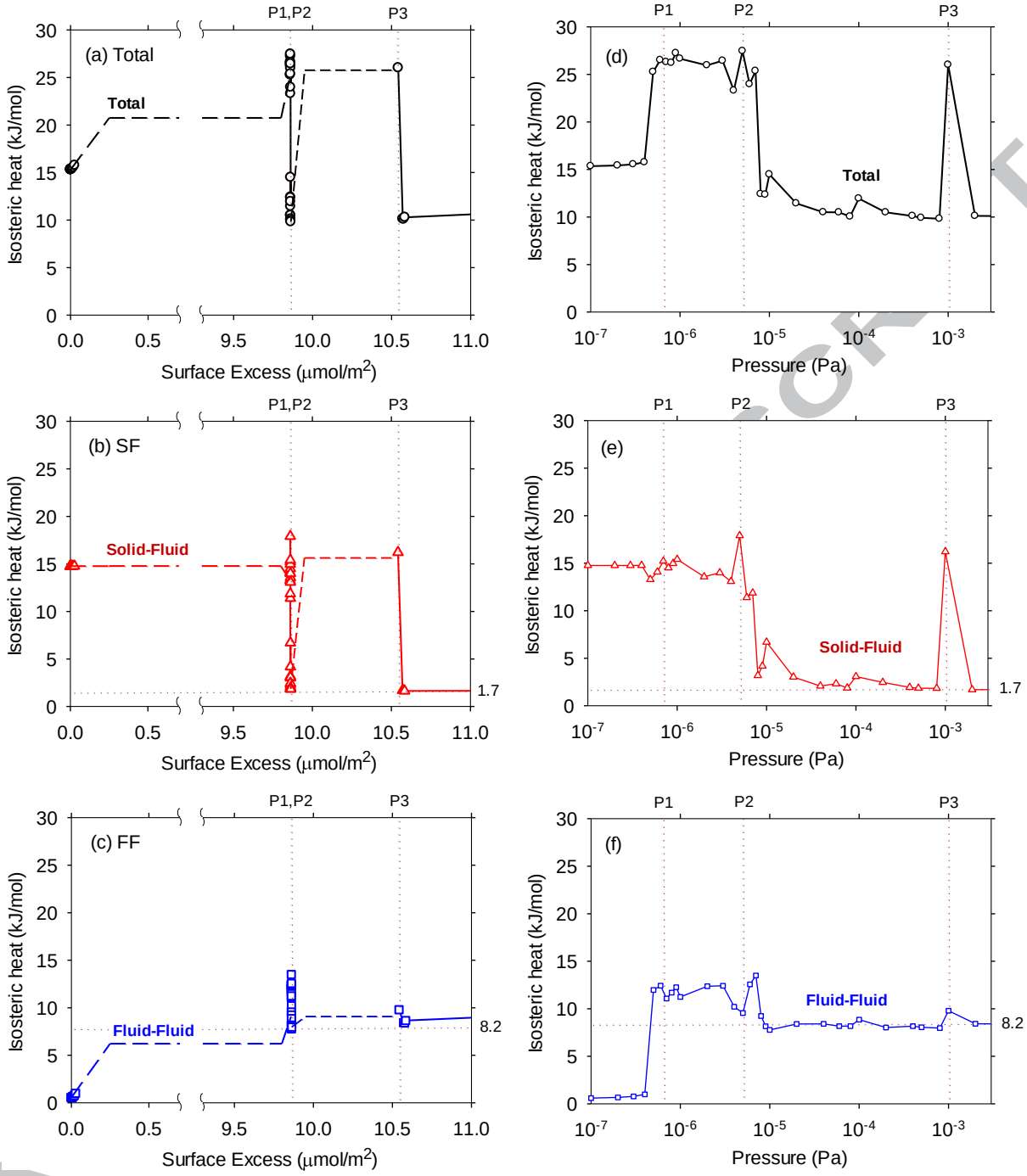

Figure 8 - *GCMC* simulated isosteric heat against loading for xenon at 65 K (shown as solid lines). The region of constant isosteric heats (total, *SF* and *FF*), shown as a dashed line, are obtained using *MCE* (see text). The scales are magnified to focus on the gas-like region (0-0.3 μmol/m^2) and the monolayer coverage region (9.7-11 μmol/m^2): (a) total isosteric heat and its decomposition into (b) solid-fluid contribution and (c) fluid-fluid contribution. The isosteric heat profile within the region of constant surface excess between Point *P1* and *P3* is plotted against pressure: (d) total isosteric heat and its decomposition into (e) solid-fluid contribution and (f) fluid-fluid contribution.

Once the 2D-condensation (G-S) has reached completion, each new molecule will interact with an increasing number of neighbouring molecules: when the first adsorbate layer is completed, there are six neighbouring molecules on average at *Point P1*, where the isosteric heat (26.3 kJ/mol) is the sum of the *SF* contribution of 15 kJ/mol and the *FF* contribution. The *FF* contribution of 12.26 kJ/mol, comes from six pairwise nearest neighbour interactions $\left(6\times 1.89\ \text{kJ/mol} = 11.3\ \text{kJ/mol}\right)$ plus interactions with molecules in distant shells. The variation of heat released within this region of constant surface excess (*i.e.* between *Points P1* and *P3*) is better seen in the plot of the isosteric heat and its *SF* and *FF* contributions versus pressure (*Figure 8*d, e, f) which shows a maximum at *Point P2*. At this point, the *SF* contribution increases to 18 kJ/mol because some molecules in the first layer migrate to the centres of the carbon hexagons, while most molecules in the first layer remain out-of-registry with the graphite surface as seen from the 2D-RDD in *Section* 3.1.3. Beyond this maximum, the isosteric heat decreases sharply because molecules begin to adsorb into the second layer. This decrease is then followed by a discontinuity in the isosteric heat curve between the transition region of 10-10.5μmol/m^2. During this transition, the *MCE* simulation (dashed lines) shows a constant heat region, typically the case for a first order transition, which is also observed across the *G-S* transition at *P1*. The constant heat indicates that the existing molecules migrate to the centres of carbon hexagons to accommodate new molecules adsorbed into the first adsorbate layer during the *IC-C* transition.

In *Figure* 10a, b, we have decomposed the isosteric heat into the contributions from the first and second layers to reveal the specific contributions from the second layer. For loadings less than at *Point P2* (where the first adsorbate layer is in *IC*-packing), only the first layer contributes to the isosteric heat. Immediately after *Point P2*, the contributions from the *SF* and *FF* interactions decrease sharply to 1.7 kJ/mol and 8 kJ/mol, respectively (*Figure 8*e, f). This corresponds to the onset of the second layer. 1.7 kJ/mol is the *SF* potential energy of a molecule in the second layer and 8 kJ/mol is the ensemble average energy of the *FF* interactions of molecules adsorbing into the second layer, which comes from interactions of a molecule with three molecules in the first layer and six neighbours in the first layer.

Point P3, is the point where the first adsorbate layer undergoes a transition from *IC*- to the *C*-packing and the *SF* contribution to the isosteric heat increases steeply to 16.2 kJ/mol. This value of *SF* energy is higher than the isosteric heat at zero loading (15 kJ/mol) which indicates that molecules enter the first adsorbate layer at the transition to *C*-packing. This

observation is further confirmed by an increase in the *FF*-contribution in the first adsorbate layer (*Figure* 10). Interestingly, at the same time there is a sharp decrease in the *FF* contribution in the second layer, suggesting that molecules migrate from the second layer to the first layer to facilitate the transition from the *IC*-packing to the *C*-packing in the first layer. Since the gain in the *FF* contribution in the first layer almost offsets the loss by the second layer, the total heat contributed by *FF* interaction is relatively constant (see *Figure* 8c) during the transition. The heat contributed by *FF* interactions at *Point P3* is less than that at *Point P1* because, prior to their migration into the first layer, molecules in the second layer have three neighbours, and when they enter the first layer, they experience additional interactions with three additional neighbours (*Figure* 10a). After the first adsorbate layer has achieved C-packing at *Point P3*, molecules enter the second layer, as indicated by the increase in the *FF* contribution in the second layer while the *FF* contribution of the first layer to the isosteric heat decreases.

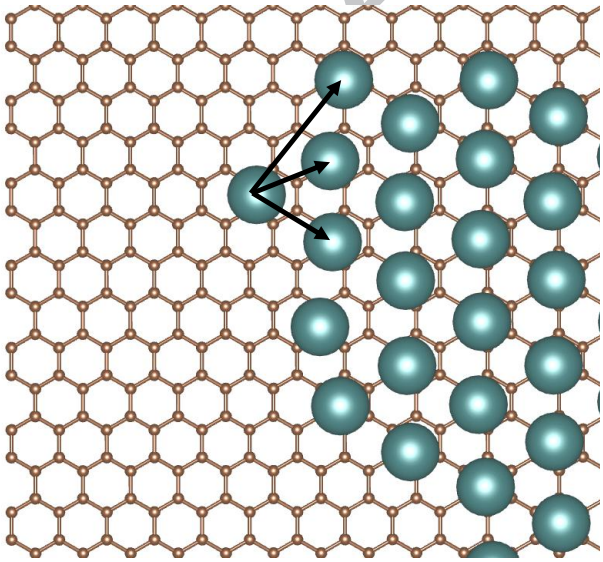

Figure 9 - A schematic representation of the boundary growth where one molecule is added to the edge of a group of adsorbed molecules during condensation (see text).

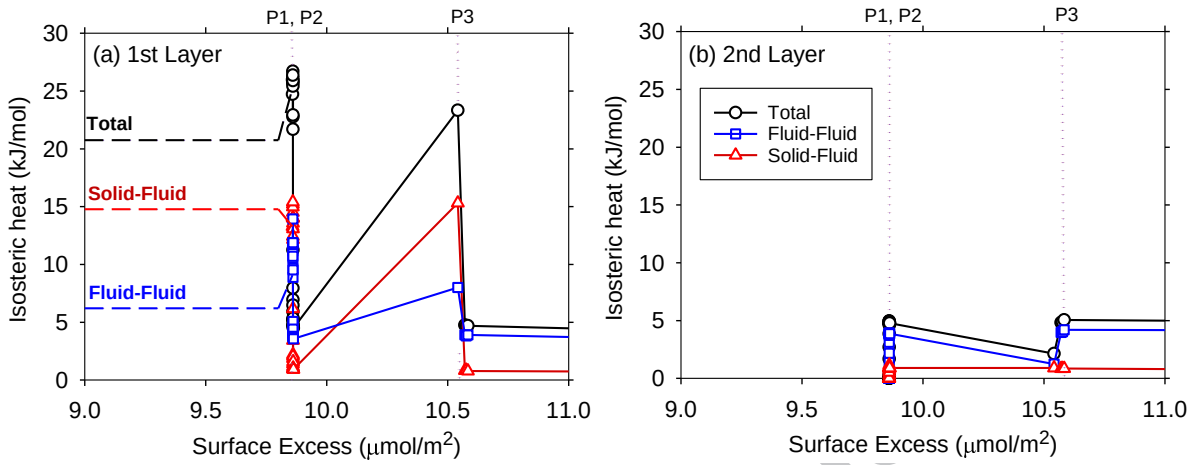

Figure 10 – *GCMC* simulated isosteric heat of xenon at 65K decomposed into contribution (a) by the first layer and (b) by the second layer.

3.1.2 Adsorption of xenon at 105K

Adsorption of xenon on graphite at 105K (between the 2D-triple and critical points), exhibits two transitions: (1) a gas-to liquid (*G*-*L*) transition and (2) a liquid-to-solid (*L*-*S*) transition. *Figure* 11 presents the simulated isotherm and the experimental data [12].

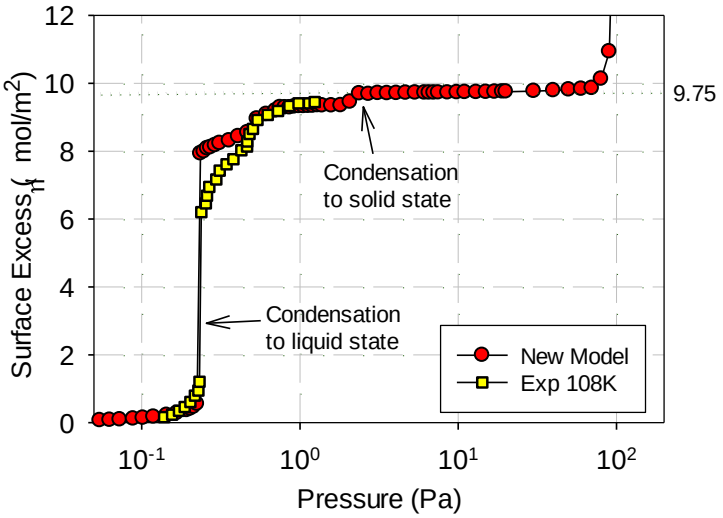

Figure 11 - Simulated adsorption isotherm of xenon at 105K and the experimental data at 108K from Thomy and Duval [4].

As seen in *Figure* 11, the simulation result successfully describes the experimental *G-L-S* transitions in the sub-monolayer coverage before the onset of the second layer. The surface excess at the *IC* packing for xenon at the monolayer coverage is 9.8 μmol/m^2, which is in good agreement with experimental results [5].

In *Figure* 12 we show the isotherms decomposed into the contributions from the first, second and third layers. The onset of the second layer begins at *Point P3* by way of a 2D-condensation to an *IC*-packed layer and, interestingly, at the same time, the first adsorbate layer undergoes a transition from *IC*-packing to *C*-packing. This is confirmed by the density distributions discussed in *Section* 3.1.3.

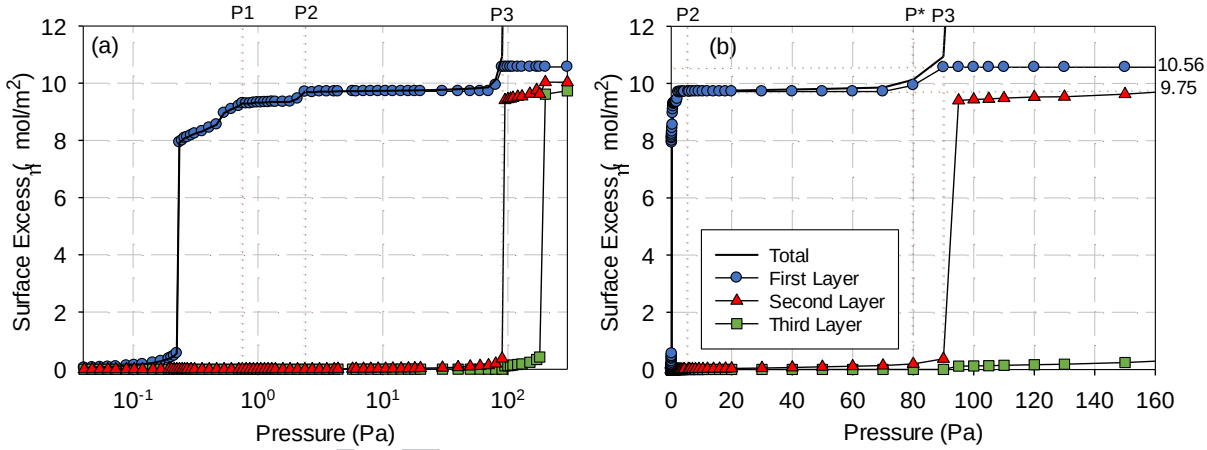

Figure 12 simulated adsorption isotherm of xenon at 105K and the contributions from the first, second and third layers: (a) log-scale; (b) linear scale.

The simulated isosteric heat versus loading at 105K is shown in *Figure* 13, and is in excellent agreement with experiment [12]. The maximum isosteric heat is well-reproduced at *Point P1* where the first adsorbate layer approaches *IC*-packing [12].

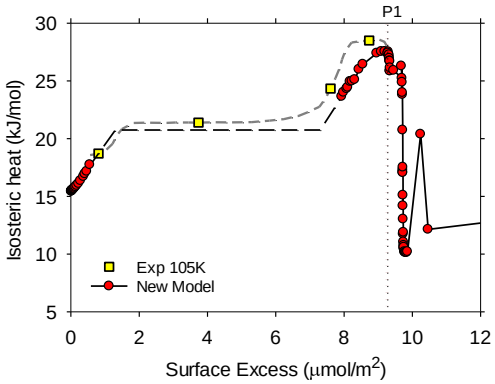

Figure 13 - The simulated isosteric heat profile of xenon at 105K and experimental data at 110K [50].

Across the 2D-condensation in the first adsorbate layer, from a gas to a liquid state, the simulated isosteric heat is constant, as shown by a constant contribution from *FF* interactions (*Figure 14*c). The liquid adsorbate grows by the boundary growth mechanism discussed earlier for adsorption at 65K, and is in perfect agreement with the experimental data of Thomy and Duval [50]. To understand the energetics of the adsorption mechanism we have decomposed the isosteric heat into contributions from *SF* and *FF* interactions as shown in *Figure* 14b, c respectively.

After the 2D-condensation to the liquid state at around 8 μmol/m^2, the first layer becomes denser to achieve an *IC*-packing at *Point P1* (shown in *Figure* 14), where the contribution from the *FF* interactions is about 13 kJ/mol, from six interacting molecules per molecule. After this point contributions from both *SF* and *FF* interactions decrease, giving rise to a cusp in the isosteric heat curve. This is due to adsorption in the second layer, because entropy favours adsorption in the second layer to adsorption into the dense first adsorbate layer. However, when the chemical potential is increased, molecules enter the first adsorbate layer, giving a spike in the isosteric heat at *Point P2*, with contributions from both *SF* and *FF* interactions. At this point, the first adsorbate layer forms an imperfect *IC* packing of density 9.7 μmol/m^2.

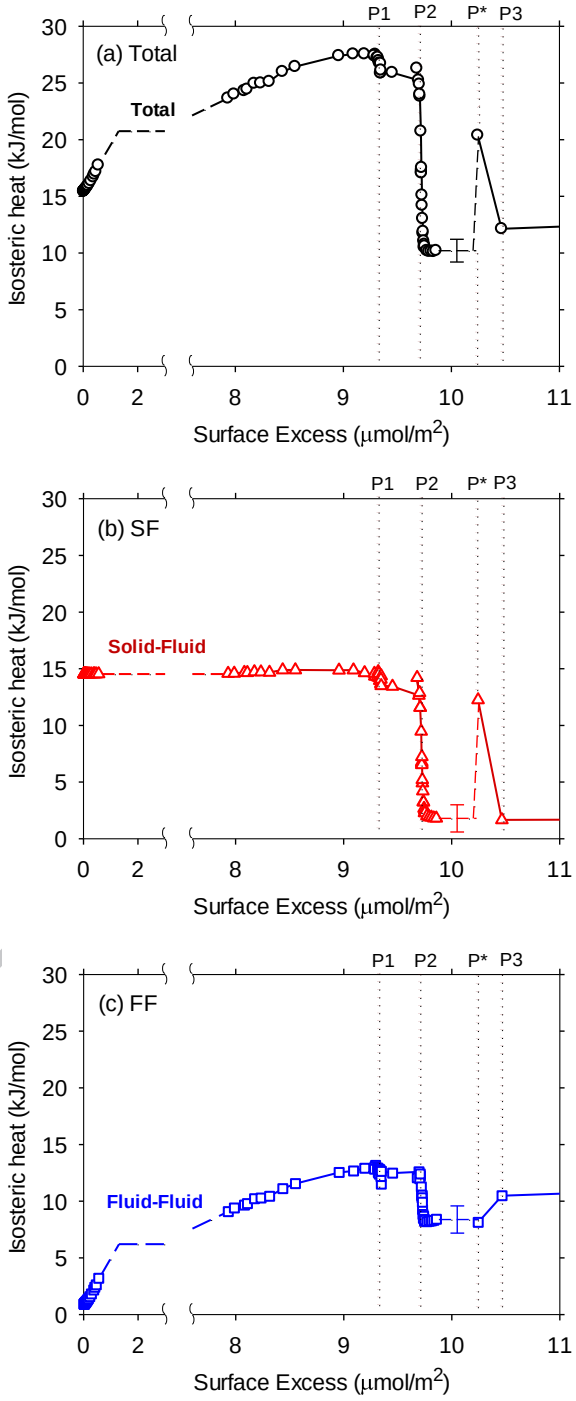

Figure 14 – A magnified view of the *GCMC* simulated isosteric heat profile for xenon adsorption on graphite at 105K in the gas-like region (0-2 μmol/m^2) and in the complete monolayer coverage region (7.5-11 μmol/m^2): (a) simulated total isosteric heat and its decomposition into contributions from (b) *SF* interactions and (c) *FF* interactions. The region of constant isosteric heats (total, *SF* and *FF*), shown as a dashed line, are obtained using *MCE*.

Beyond *Point P2*, molecules enter the second layer and therefore both *SF* and *FF* contributions to the heat decrease strongly as shown in *Figure* 14. As the second layer is progressively filled, some molecules from the second layer migrate into the first adsorbate layer which undergoes a transition to *C* packing at *Point P3*, giving a heat spike in the *SF* contribution at *Point P**. If a molecule enters the first adsorbate layer, its *SF* interaction would be expected to contribute 15 kJ/mol to the isosteric heat, but in fact, the contribution to the heat is only 12kJ/mol. This is because the isosteric heat is the ensemble average of adsorption of new molecules in the first layer as well as in the second layer. The isosteric heat across the transition region of *Point P2* to *P** is determined by *MCE* simulation and it indicates that the molecules are adsorbed onto the second layer at pressures less than *P**. The contribution from the total *FF* interactions to the isosteric heat seems to be constant. This is because the amount adsorbed into the second layer is so low that molecules in the second layer are so far apart that their FF interaction is weak and also because some of them move into the first layer, resulting in a constant isosteric heat shown as the dashed line in *Figure* 14.

3.1.3 Local Properties Analysis

The various transitions discussed in the previous sections are corroborated by the local density distribution (*LDD*) and the 2D-radial density distribution (*2D-RDD*) for the first adsorbate layer.

Local Density Distribution (LDD)

The local density distribution in *Figure 15* shows the increase in the density of the first adsorbate layer during the *IC-C* transition at 65K and 105K, confirming that molecules enter the first layer to form a *C* packing. As shown in *Figure 15*b at 105K, xenon forms a *C* packed layer after the second layer has been formed, in contrast to adsorption at 65K where *C*-packing of the first adsorbate occurs when the second layer is nearly empty.

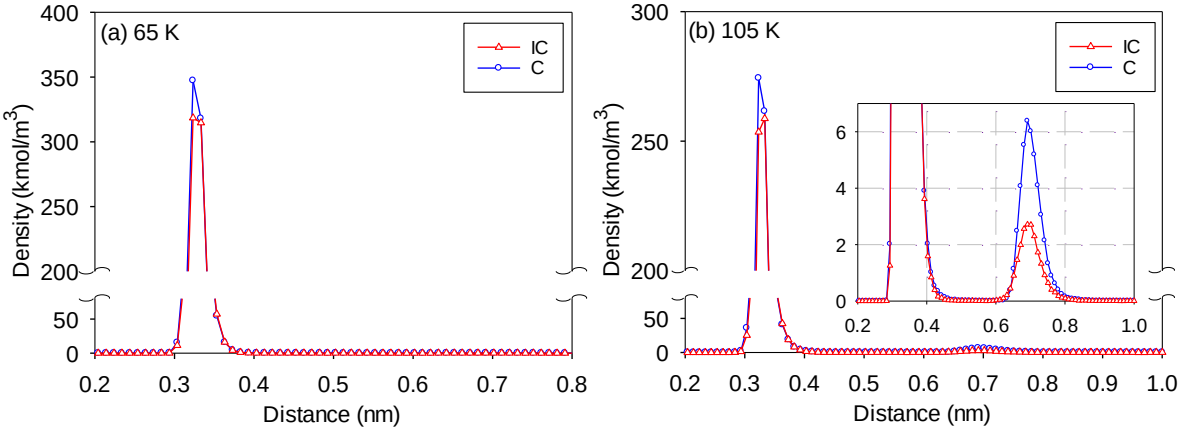

Figure 15 - Simulated local density distributions for xenon adsorbed on graphite at a) 65 K and b) 105 K.

Evolution of the 2D-RDD in the first and second layers during the IC-C transition

Figure 16a, b show the *2D-RDD* in the first and second layers before and after the transition. The *2D-RDD* of the *IC*-packing has a solid-like pattern, as characterized by the sharp and structured peaks. After *C*-packing has occurred, the peaks become sharper at 65K and at 105K, and the average distance between neighbouring molecules is 0.426 nm, which is the lattice spacing in a *C*-packed layer. This separation is closer than the distance of the first peak of the *IC*-packing, which is 0.438 nm. The *C*-packing is further confirmed by the position of the peaks in the second and higher shells, all of which correspond to the separations for a perfect commensurate structure (see *Appendix* C). At 65K, the *2D-RDD* of the 2nd layer reaffirms that this layer remains in *IC*-packing after the transition (at *Point P4* in *Figure 6b*).

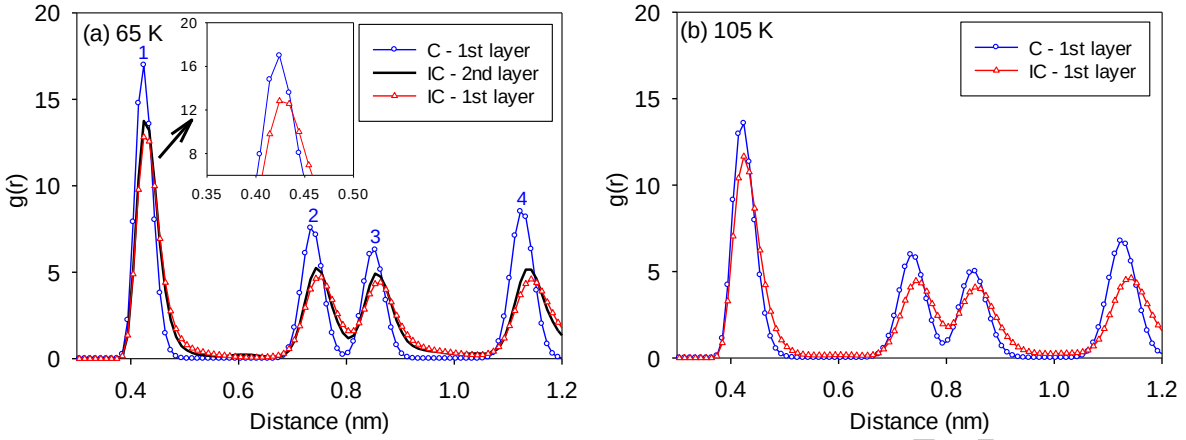

Figure 16 - 2D Radial density distribution of xenon on graphite during the *IC*-*C* transition for: (a) 65 K and (b) 105 K

3.2 Adsorption of Neon on graphite

3.2.1 Adsorption of Neon at 25 K

Neon has a much smaller diameter than the commensurate lattice spacing and its interaction energy with the graphite surface is weaker; hence it is unable to form a *C* packed layer. The simulated isotherm of neon adsorption on graphite at 25K is shown in *Figure* 17a, and is in good qualitative agreement with experiment [26]. Both the simulated and the experimental isotherms suggest that 25K is above the 2D-critical temperature, which is reported to be 15.8K [42]. Hence, the isotherm exhibits a transition from the supercritical state to solid packing.

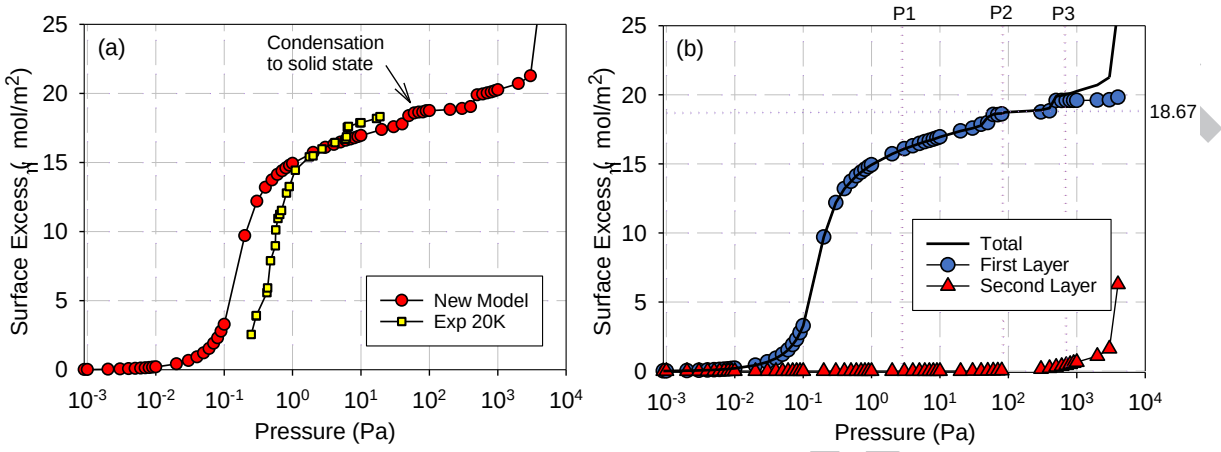

Figure 17 – (a)*GCMC* simulated adsorption isotherm of neon on graphite at 25K using the new model in comparison to experimental data at 20K [9], (b) contributions from first and second layer

At the end of the transition, the adsorbate density from the simulation results is 18.7 μmol/m^2, which is less than 19.3 μmol/m^2, which is the theoretical density of a perfect *IC*-packing, but is in perfect agreement with experiment [12]. To gain further insight, we decomposed the isotherms into contributions from the first and second layers as shown in *Figure* 17b. This figure shows that the first adsorbate layer undergoes a transition from the supercritical state to *IC*-packing before the onset of the second layer. Once adsorption in the second layer has started, the first layer densifies to an *IC*-packed layer.

The normalised simulated isosteric heat of neon adsorption at 25K shows good qualitative agreement with the experimental isosteric heat at 24K [35] (see *Figure* 18). However, the experimental result does not show a spike at loadings close to monolayer coverage which could be due to the difficulty in measuring the very small amount of heat released by the calorimetric technique.

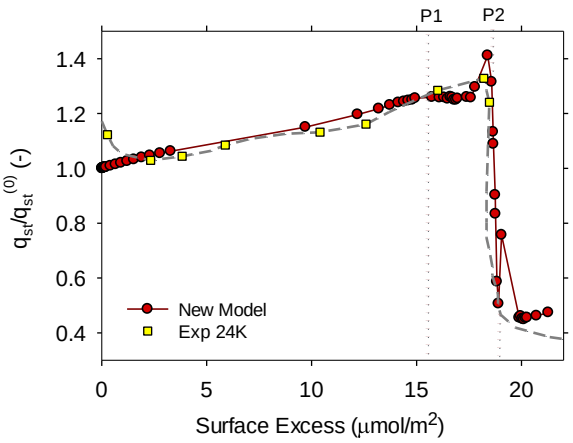

Figure 18 - The normalised simulated isosteric heat of neon at 25K in comparison with experimental data at 24K [51]

Figure 19 shows the isosteric heat decomposed into contributions from the *SF* and *FF* interactions. For loadings below *Point P1*, where the first adsorbate layer is in a supercritical state, the contribution from the *FF* interactions increases (because of the increase in the number of neighbouring molecules) while that from the *SF* interactions decreases slightly. This suggests that molecules move away from the centres of the carbon hexagons to maximise the *FF* interactions. At *Point P2* when the chemical potential is sufficient for more molecules to adsorb onto the surface, the first adsorbate layer undergoes a transition to *IC*-packing, and there is a spike in the isosteric heat curve. These molecules facilitate rearrangement of the first adsorbate layer, resulting in an increase in the contribution of the *FF* interactions because of the shorter separation distances between neighbouring molecules. The peak in the contribution of the *FF* interactions is close to 2 kJ/mol, which comes from six neon-neon interactions at their minimal potential distance (each pair interaction is 0.28 kJ/mol). Beyond *Point P2*, molecules are added to the second layer and there is a sharp drop in the contributions from both *SF* and *FF* interactions until a cusp is formed in the isosteric heat plot. At this point, the chemical potential is sufficient for more molecules to adsorb into the first adsorbate layer. This results in an ordering transition in the first layer producing a spike in the isosteric heat at *Point P3*. The increase in density in the first adsorbate layer and the steep increase in the contribution from the *SF* interactions suggest that molecules in the first adsorbate layer migrate towards the centre of the carbon hexagons.

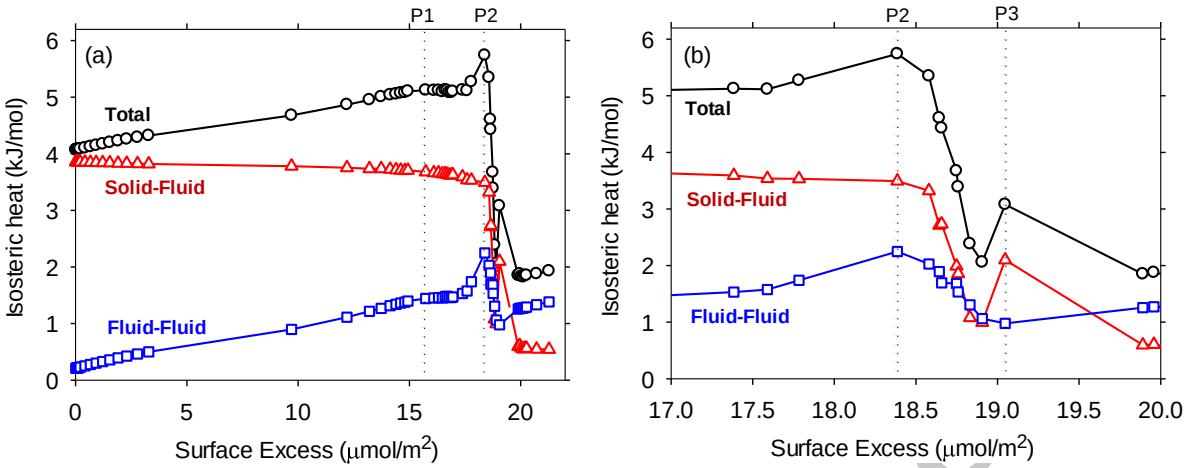

Figure 19 – *GCMC* simulated isosteric heat of neon at 25 K decomposed into *SF* and *FF* contributions a) general view and b) magnified view for loadings 17-20 μmol/m^2

3.3 The generic isosteric heat of nobles gases (Ne, Kr, Ar, Xe) undergoing *C-IC* transitions

To complete our investigation into the phenomenon of structural ordering of adsorption of simple gases, we provide, in this section, a generic isosteric heat profile of adsorption of noble gases and simple gases (examples of N_2 and CH_4) on graphite as a function of temperature. This generic isosteric heat profile describes all the features observed in the experiments and show characteristics of the ordering transition in these adsorbates in the monolayer coverage region.

In a typical isosteric heat profile, an *IC-C* or *C-IC* transition is identified by a heat spike occurring in the following sequence: a first dense-phase peak (*Point A*) - a cusp (*Point B*) - a heat spike (*Point C*). For noble and simple gases adsorbed on graphite, the generic isosteric heat profiles for a range of temperatures are shown in *Figure* 20:

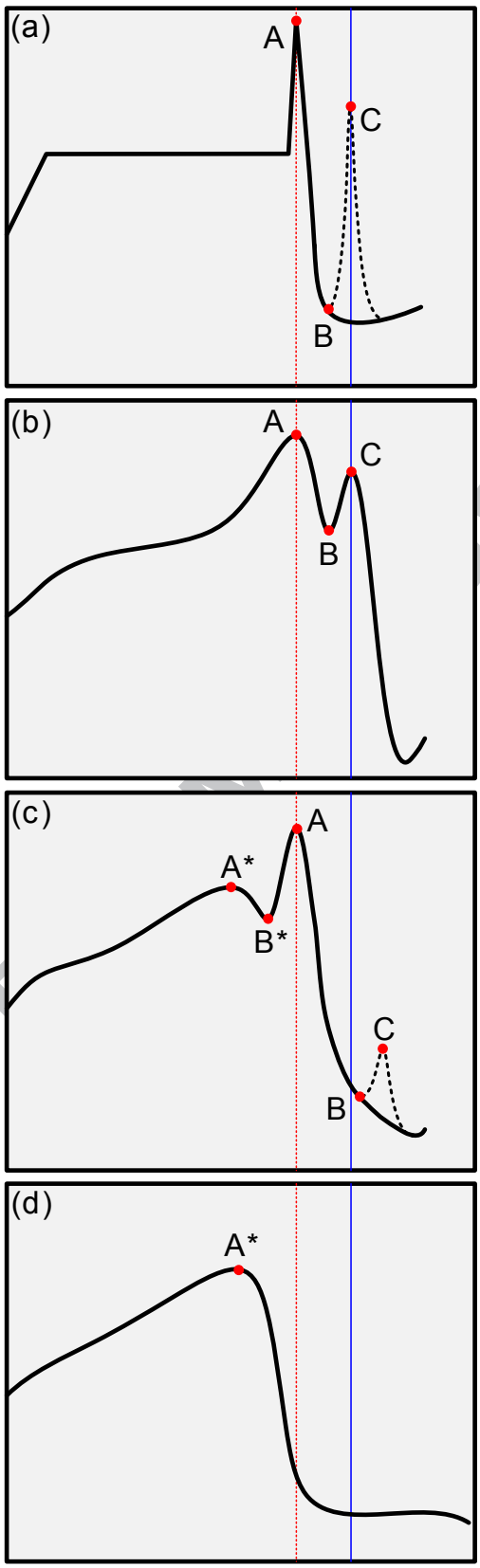

Figure 20 - Generic isosteric heat profile at different temperatures (see text). The Red line and blue line mark the densities of the first and second dense phase during the course of adsorption.

a) *Case A:* $T < T_t$. The region of constant isosteric heat represents the 2D-condensation to solid state of the first adsorbate layer, followed by a maximum heat released at the first dense-phase peak (*Point A*), corresponding to a complete solid-state monolayer where each adsorbed molecule interacts with six neighbouring molecules releasing a maximum heat of $q_{st} = q_{st}^{(0)} + 6\frac{\varepsilon_{ff}}{k_B}$. The 2D-solid first layer can either be *C* or *IC* depending on the size of the adsorbate. The ensuing sharp drop in the isosteric heat immediately after *Point A* indicates the addition of molecules into the second layer. A sharp peak at *Point C* following the decline after *Point A* could occur depending on the ability of the molecules in the first layer to undergo a transition from *C* to *IC* packing, as in the case of krypton or methane or from *IC* to *C*, as in the case of xenon.

b) *Case B:* $T_t < T < T_c$. The region of constant isosteric heat represents the condensation to a 2D-liquid state in the first adsorbate layer. This liquid phase becomes denser as indicated by the moderate increase in the isosteric heat towards the first dense-phase peak (*Point A*) where condensation to the solid state occurs. The maximum heat released occurs at either *C* or *IC* packing. Beyond the solid-state condensation, the isosteric heat decreases as molecules prefer to adsorb into the second layer until the chemical potential is high enough (*Point B*) to squeeze molecules into the first layer to order it to form a denser packing (*C* or *IC*). This corresponds to a heat spike (*Point C*).

c) *Case C:* $T > T_c$. At temperature above T_c, the first adsorbate layer is in a 2D-supercritical state. The isosteric heat increases gradually as the first layer is filled to completion at *Point* A^*. When the chemical potential is high enough (*Point* B^*) molecules enter the first adsorbate layer and a transition to a 2D-solid state occurs (*Point A*). The heat at *Point A* is higher than *Point A** because the inter-particle separation distance approaches the minimum potential distance to maximise the *FF* interactions. The isosteric heat then declines due to adsorption into the second layer until the chemical potential has reached *Point B* beyond which the first adsorbate layer undergoes a transition at *Point C* to form either the *C* or *IC* packing, resulting in a spike. This spike (*Point C*) shifts to higher loadings at higher temperatures because a higher chemical potential is required to counter an increase in entropy (temperature). The height of the heat spike gradually diminishes because its contribution towards the total isosteric heat is masked by the adsorption of molecules in the second or higher layers.

d) *Case D:* $T >> T_c$. At temperature much higher than T_c, there is no 2D-solid phase. Only the first dense-phase peak (*Point* A^*) is observed when the monolayer coverage is reached. The

heat released due to the ordering transition in the first layer is masked by the heat released due to adsorption onto higher layers.

4 Conclusion

We have made extensive simulations of adsorption on a *CA* graphite model for a range of temperatures to study the ordering transitions of xenon and neon whose sizes and interaction energies lie at opposite extremes for the noble gases. The simulation results using the *CA* graphite model describe well the transition from *IC* to *C* packing for xenon and the transition from fluid to *IC* packing for neon, all of which are supported with experimental findings. We conclude that the ability of adsorbate molecules to form *IC* or *C* packing depends on the separation at the minimum of the intermolecular potential relative to the commensurate graphite lattice spacing λ. Krypton, methane and nitrogen undergo a *C*-*IC* ordering transition since their minimum intermolecular potential distance is close to λ. Xenon experiences an *IC*-*C* transition since its minimum intermolecular potential separation is larger than λ while argon and neon can only form an *IC* packing since their collision diameters are smaller than λ. The ordering transitions of adsorbate molecules are reflected in the isosteric heat curves and a generic heat profile was provided for a range of different temperatures.

Acknowledgement: This work is supported by the Australian Research Council (DP16013540)

Reference

1. Prasetyo, L., S. Tan, Y. Zeng, D.D. Do, and D. Nicholson, *An improved model for N2 adsorption on graphitic adsorbents and graphitized thermal carbon black—The importance of the anisotropy of graphene.* The Journal of Chemical Physics, 2017. **146**(18): p. 184702.
2. Mowforth, C.W., T. Rayment, and R.K. Thomas, *Long-period commensurate structures near the incommensurate-commensurate phase transition in xenon layers adsorbed on graphite observed by X-ray diffraction.* Journal of the Chemical Society, Faraday Transactions 2: Molecular and Chemical Physics, 1986. **82**(10): p. 1621-1634.
3. Morishige, K., K. Kawamura, M. Yamamoto, and I. Ohfuji, *Capillary condensation of xenon on exfoliated graphite.* Langmuir, 1990. **6**(8): p. 1417-1421.
4. Thomy, A., X. Duval, and J. Regnier, *Two-dimensional phase transitions as displayed by adsorption isotherms on graphite and other lamellar solids.* Surface Science Reports, 1981. **1**(1): p. 1-38.
5. Thomy, A. and X. Duval, *Adsorption of Simple Molecules on Graphite .3. Passage of First Layer by Three Sucessive States.* Journal De Chimie Physique Et De Physico-Chimie Biologique, 1970. **67**(6): p. 1101-1110.
6. Suzanne, J., J. Coulomb, and M. Bienfait, *Auger electron spectroscopy and leed studies of adsorption isotherms: Xenon on (0001) graphite.* Surface Science, 1973. **40**(2): p. 414-418.
7. Suzanne, J., J. Coulomb, and M. Bienfait, *Transition bidimensionnelle du premier ordre; cas du xénon adsorbé sur la face (0001) du graphite.* Surface Science, 1974. **44**(1): p. 141-156.
8. Calisti, S. and J. Suzanne, *Orientational epitaxy of an incommensurate neon monolayer adsorbed on graphite.* Surface Science Letters, 1981. **105**(1): p. L255-L259.
9. Thomy, A., X. Duval, and J. Regnier, *Mobile-immobile transition during formation at 20.4 degrees kelvin of first adsorption layer of neon on graphite.* Comptes rendus hebdomadaires des seances de l academie des sciences serie c, 1969. **268**(16): p. 1416-&.
10. Hanono, F., C. Gatts, and E. Lerner, *Multilayer isotherms of neon adsorbed on exfoliated graphite.* Journal of low temperature physics, 1985. **60**(1-2): p. 73-84.
11. Duval, X. and A. Thomy, *The interpretation of Krypton adsorption isotherms on exfoliated graphite.* Carbon, 1975. **13**(3): p. 242-243.
12. Larher, Y., *Triple point of first monomolecular layer of krypton adsorbed on the cleavage face of graphite.* Journal of the Chemical Society-Faraday Transactions I, 1974. **70**(2): p. 320-329.
13. Thomy, A. and X. Duval, *Adsorption Of Simple Molecules On Graphite.2. Variation Of Adsorption Potential As Function Of Number Of Adsorbed Layers.* Journal De Chimie Physique Et De Physico-Chimie Biologique, 1970. **67**(2): p. 286-&.
14. Rouquerol, J., S. Partyka, and F. Rouquerol, *Calorimetric evidence for a bidimensional phase change in the monolayer of nitrogen or argon adsorbed on graphite at 77 K.* Journal of the Chemical Society, Faraday Transactions 1: Physical Chemistry in Condensed Phases, 1977. **73**: p. 306-314.
15. Grillet, Y., F. Rouquerol, and J. Rouquerol, *Two-dimensional freezing of nitrogen or argon on differently graphitized carbons.* Journal of Colloid and Interface Science, 1979. **70**(2): p. 239-244.

16. Horikawa, T., Y. Zeng, D.D. Do, K.-I. Sotowa, and J.R. Alcántara Avila, *On the isosteric heat of adsorption of non-polar and polar fluids on highly graphitized carbon black.* Journal of Colloid and Interface Science, 2015. **439**: p. 1-6.
17. Diehl, R. and S. Fain Jr, *Adsorption of nitrogen molecules on graphite for 31< T< 52 K: The fluid-to-commensurate-solid transition, multilayer condensation, and the pressure–temperature phase diagram.* The Journal of Chemical Physics, 1982. **77**(10): p. 5065-5072.
18. Larher, Y., *''Phase transitions''between dense monolayers of atoms and simple molecules on the cleavage face of graphite, with particular emphasis on the transition of nitrogen from a fluid to a registered monolayer.* The Journal of Chemical Physics, 1978. **68**(5): p. 2257-2263.
19. Do, D. and H. Do, *Effects of potential models on the adsorption of carbon dioxide on graphitized thermal carbon black: GCMC computer simulations.* Colloids and Surfaces A: Physicochemical and Engineering Aspects, 2006. **277**(1): p. 239-248.
20. Piper, J., J. Morrison, and C. Peters, *The adsorption of carbon monoxide on graphite.* Molecular Physics, 1984. **53**(6): p. 1463-1480.
21. Inaba, A., Y. Koga, and J.A. Morrison, *Multilayers of methane adsorbed on graphite.* Journal of the Chemical Society, Faraday Transactions 2: Molecular and Chemical Physics, 1986. **82**(10): p. 1635-1646.
22. Piper, J. and J. Morrison, *Heats of adsorption of methane multilayers on graphite.* Physical Review B, 1984. **30**(6): p. 3486.
23. Do, D. and H. Do, *Effects of potential models on the adsorption of ethane and ethylene on graphitized thermal carbon black. Study of two-dimensional critical temperature and isosteric heat versus loading.* Langmuir, 2004. **20**(25): p. 10889-10899.
24. Inaba, A. and J.A. Morrison, *Ethylene on graphite: Heats of adsorption and phase diagram.* Phys. Rev. B, 1986. **34**(5): p. 3238-3242.
25. Do, D. and H. Do, *Adsorption of benzene on graphitized thermal carbon black: Reduction of the quadrupole moment in the adsorbed phase.* Langmuir, 2006. **22**(3): p. 1121-1128.
26. Fan, C., D. Do, D. Nicholson, J. Jagiello, J. Kenvin, and M. Puzan, *Monte Carlo simulation and experimental studies on the low temperature characterization of nitrogen adsorption on graphite.* Carbon, 2013. **52**: p. 158-170.
27. Zeng, Y., K. Horio, T. Horikawa, K. Nakai, D. Do, and D. Nicholson, *On the evolution of the heat spike in the isosteric heat versus loading for argon adsorption on graphite-A new molecular model for graphite & reconciliation between experiment and computer simulation.* Carbon, 2017. **122**: p. 622-634.
28. Steele, W.A., *The physical interaction of gases with crystalline solids: I. Gas-solid energies and properties of isolated adsorbed atoms.* Surface Science, 1973. **36**(1): p. 317-352.
29. Bruch, L. and A.D. Novaco, *Stability analysis of the commensurate monolayer solid of xenon/graphite.* Physical Review B, 2008. **77**(12): p. 125435.
30. Hamichi, M., A. Faisal, J. Venables, and R. Kariotis, *Lattice parameter and orientation of xenon on graphite at low pressures.* Physical Review B, 1989. **39**(1): p. 415.
31. Nuttall, W., K. Fahey, M. Young, B. Keimer, R. Birgeneau, and H. Suematsu, *A synchrotron X-ray diffraction study of the structural phase behaviour of multilayer xenon on single-crystal graphite.* Journal of Physics: Condensed Matter, 1993. **5**(44): p. 8159.

32. Schabes-Retchkiman, P. and J. Venables, *Structural studies of xenon and krypton solid monolayers on graphite using transmission electron diffraction.* Surface Science, 1981. **105**(2-3): p. 536-564.
33. Hong, H., C. Peters, A. Mak, R. Birgeneau, P. Horn, and H. Suematsu, *Synchrotron x-ray study of the structures and phase transitions of monolayer xenon on single-crystal graphite.* Physical Review B, 1989. **40**(7): p. 4797.
34. Hong, H., C. Peters, A. Mak, R. Birgeneau, P.M. Horn, and H. Suematsu, *Commensurate-incommensurate and rotational transitions of monolayer xenon on single-crystal graphite.* Physical Review B, 1987. **36**(13): p. 7311.
35. Huff, G. and J. Dash, *Phases of neon monolayers adsorbed on basal plane graphite.* Journal of Low Temperature Physics, 1976. **24**(1): p. 155-174.
36. Ravikovitch, P.I., A. Vishnyakov, and A.V. Neimark, *Density functional theories and molecular simulations of adsorption and phase transitions in nanopores.* Physical Review E, 2001. **64**(1): p. 011602.
37. Phadungbut, P., V.T. Nguyen, D.D. Do, D. Nicholson, and C. Tangsathitkulchai, *On the phase transition in a monolayer adsorbed on graphite at temperatures below the 2D-critical temperature.* Molecular Simulation, 2015. **41**(5-6): p. 446-454.
38. Nguyen, V.T., D. Do, and D. Nicholson, *Monte Carlo simulation of the gas-phase volumetric adsorption system: effects of dosing volume size, incremental dosing amount, pore shape and size, and temperature.* The Journal of Physical Chemistry B, 2011. **115**(24): p. 7862-7871.
39. Neimark, A.V. and A. Vishnyakov, *Gauge cell method for simulation studies of phase transitions in confined systems.* Physical Review E, 2000. **62**(4): p. 4611.
40. Widom, B., *Potential-distribution theory and the statistical mechanics of fluids.* The Journal of Physical Chemistry, 1982. **86**(6): p. 869-872.
41. Vrabec, J., J. Stoll, and H. Hasse, *A set of molecular models for symmetric quadrupolar fluids.* The Journal of Physical Chemistry B, 2001. **105**(48): p. 12126-12133.
42. Bruch, L.W., M.W. Cole, and E. Zaremba, *Physical adsorption: forces and phenomena*. 2007: Courier Dover Publications.
43. Choi, B., H. Nham, S. Kwon, J. Kim, H. Youn, and T.K. Lim, *Phase diagram of a physisorbed argon monolayer on graphite.* Journal of the Korean Physical Society, 2006. **49**(6): p. 2348-2352.
44. Kim, H.-Y. and W. Steele, *Computer-simulation study of the phase diagram of the CH 4 monolayer on graphite: Corrugation effects.* Physical Review B, 1992. **45**(11): p. 6226.
45. Carlos, W.E. and M.W. Cole, *Anisotropic He-C pair interaction for a He atom near a graphite surface.* Physical Review Letters, 1979. **43**(10): p. 697.
46. Carlos, W.E. and M.W. Cole, *Interaction between a He atom and a graphite surface.* Surface Science, 1980. **91**(1): p. 339-357.
47. Nicholson, D., *First order dispersion energy in the interaction of small molecules with graphite.* Surface science, 1984. **146**(2-3): p. 480-500.
48. Do, D., D. Nicholson, and H. Do, *On the Henry constant and isosteric heat at zero loading in gas phase adsorption.* Journal of colloid and interface science, 2008. **324**(1): p. 15-24.
49. Prasetyo, L., D.D. Do, and D. Nicholson, *A coherent definition of Henry constant and isosteric heat at zero loading for adsorption in solids – An absolute accessible volume.* Chemical Engineering Journal, 2018. **334**(Supplement C): p. 143-152.

50. Thomy, A. and X. Duval, *Adsorption de molécules simples sur graphite-I.—Homogénéité de la surface du graphite exfolié. Originalité et complexité des isothermes d'adsorption.* Journal de Chimie Physique, 1969. **66**: p. 1966-1973.
51. Antoniou, A., *The adsorption of neon on graphitized carbon in the submonolayer and multilayer region between 1.5 and 30° K.* The Journal of Chemical Physics, 1976. **64**(12): p. 4901-4911.
52. Nicholson, D. and G. Parsonage, *Computer simulation and the statistical mechanics of adsorption*. 1982, London: Academic Press.

Appendix A – Thermodynamic Properties

Surface excess

The surface excess concentration is defined as:

$$\Gamma_{ex} = \frac{N_{ex}}{L_x L_y} = \frac{\langle N \rangle - V_{acc}\rho_G}{L_x L_y} \quad (1)$$

Where N_{ex} is the excess amount adsorbed, $\langle N \rangle$ is the ensemble average of the number of particles in the simulation box, ρ_G is the bulk gas density, V_{acc} is the accessible volume (defined as the volume that is accessible to the centre of a molecule where the *SF* potential is non-positive), L_x and L_y are the box dimensions in the *x*- and *y*-directions, respectively.

Isosteric heat

In the *GCMC* ensemble, the isosteric heat was calculated from fluctuation theory [52] as:

$$q_{st} = \frac{\langle U \rangle \langle N \rangle - \langle UN \rangle}{\langle N^2 \rangle - \langle N \rangle^2} + k_B T \quad (2)$$

where *U* is the sum of the potential energies of interaction between adsorbate molecules (U_{FF}) and between adsorbate-solid adsorbent (U_{SF}), and *N* is the number of particles in the system.

To understand how various interactions contribute to the isosteric heat, we decomposed the energy term in the above equation into contributions from the *SF* and *FF* interactions. Similarly, the contributions from each layer, q_K, can be calculated from:

$$q_K = \frac{\langle U_K \rangle \langle N \rangle - \langle U_K N \rangle}{\langle N^2 \rangle - \langle N \rangle^2} \quad (3)$$

where U_K is the energy calculated as the sum of pairwise energies when two molecules reside in the same layer or half the pairwise energy if one of them is located in a different layer. The sum of contributions from all layers is thus the total isosteric heat. In a meso-canonical ensemble, the heat across the transition can be computed from the derivative of the configuration energy with respect to loading.

Local density distribution

The variation in the distance of the centre of geometry of adsorbate molecules from the surface was calculated as:

$$\rho(z) = \frac{\langle \Delta N_{z,z+\Delta z} \rangle}{L_x L_y \Delta z} \tag{4}$$

where $\langle \Delta N_{z,z+\Delta z} \rangle$ is the ensemble average of the number of molecules whose centre of geometry is located in the region bound between z and $z+\Delta z$.

Radial density distribution

The 2D-radial density distribution of Xe molecules in the first layer was calculated from:

$$\rho(r) = \frac{\langle \Delta N_{r,r+\Delta r} \rangle}{(4/3)\pi\left[(r+\Delta r)^3 - r^3\right]} \tag{5}$$

Where $\langle \Delta N_{z,z+\Delta z} \rangle$ is the average number of particles whose centres of mass are located in the first layer and in the radial bin bounded by $[r, r+\Delta r]$.

Appendix B – The effect of γ_R on the adsorption isotherms

Xenon

The effects of γ_R and anisotropy on the adsorption of xenon at monolayer coverage are explored in *Figure* 21. The choice of γ_R clearly has a significant impact on the characteristics of the 2D solid phase of the monolayer. When γ_R is negative, the adsorbate prefers the centre of the graphene hexagons because the inter-site energy barriers are higher. With γ_R = -0.54 or -1.05, the xenon monolayer exhibits an *IC-C* transition before the onset of the second layer. However, this transition was not observed in Thomy and Duval's reported isotherms [5] and is not supported by diffraction studies [30-33]. Therefore, these negative values have been rejected. The simulated isotherms are closest to experimental observation when γ_R is in the range $-0.1 \le \gamma_R \le 0$. In this work, we choose $\gamma_R = 0$.

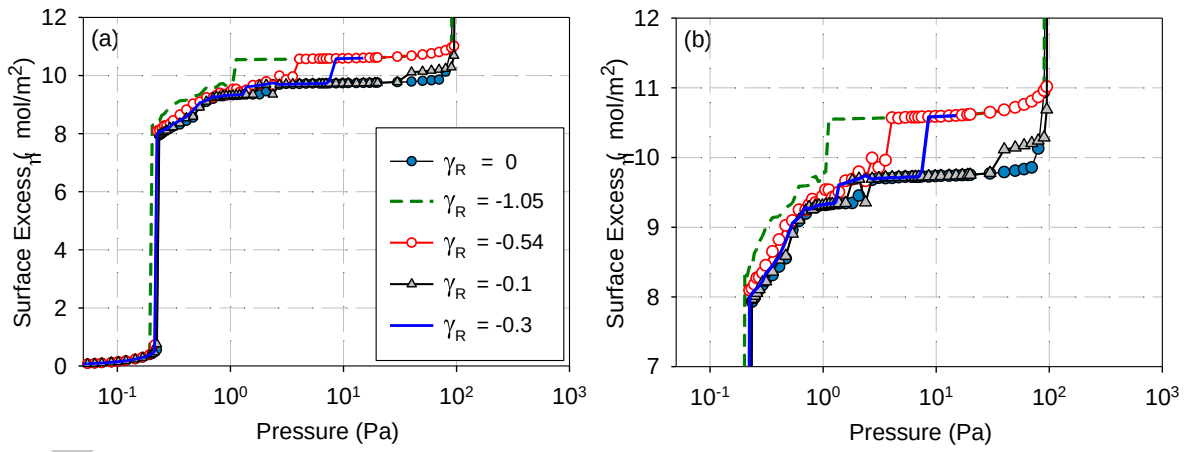

Figure 21 – (a) The effect of the choice of γ_R on the characteristics of monolayer coverage region, (b) magnification of IC-C transition region

Neon

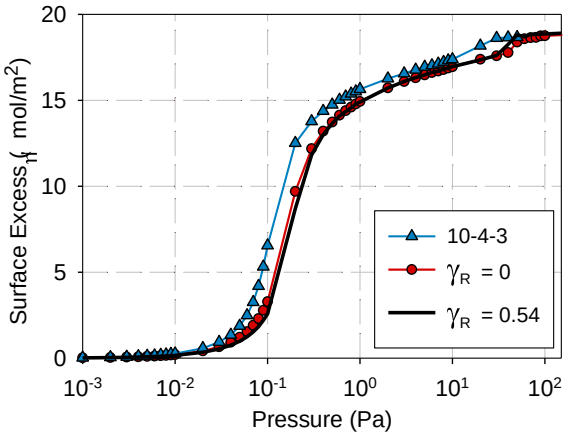

Figure 22 - Adsorption of neon at 25K: comparison of the homogeneous 10-4-3 potential model and the new model (with $\gamma_R = 0$ and $\gamma_R = 0.54$)

Appendix C – 2D Radial density distribution of a perfect commensurate phase

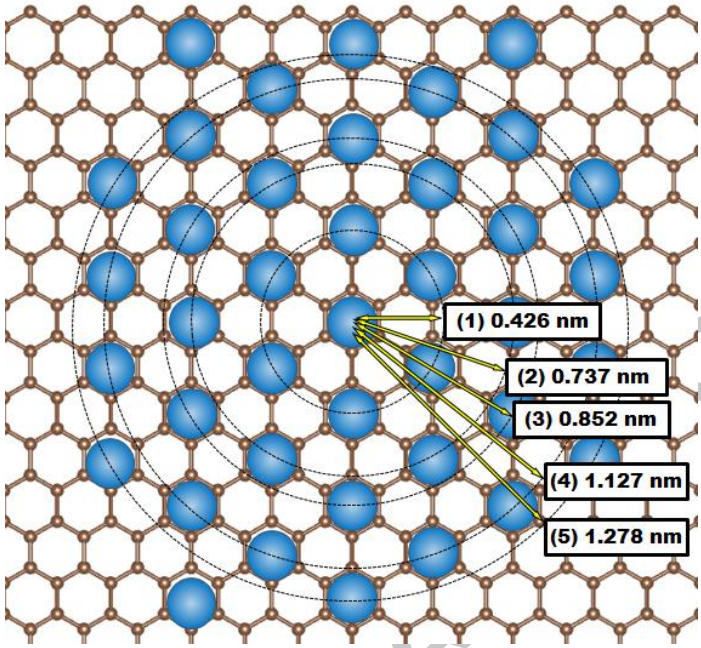

Figure 23- Schematic radial distribution for a perfect commensurate phase on a graphene plane